AGU PUBLICATIONS

Geophysical Research Letters

RESEARCH LETTER
10.1002/2017GL072539

Key Points:
- The 17 December 2016 M_w 7.9 Solomon Islands earthquake is a compound event involving intraslab and plate boundary ruptures
- Intraslab compressional faulting with M_w 7.6 ruptured from 90 to 120 km depth and coseismically triggered a M_w 7.6 plate boundary thrust
- The triggered megathrust rupture was in the area of 1971 and 1995 events, so it was approaching its failure level of strain accumulation

Supporting Information:
- Supporting Information S1

Correspondence to:
T. Lay,
tlay@ucsc.edu

Citation:
Lay, T., L. Ye, C. J. Ammon, and H. Kanamori (2017), Intraslab rupture triggering megathrust rupture coseismically in the 17 December 2016 Solomon Islands M_w 7.9 earthquake, *Geophys. Res. Lett.*, *44*, 1286–1292, doi:10.1002/2017GL072539.

Received 5 JAN 2017
Accepted 27 JAN 2017
Accepted article online 29 JAN 2017
Published online 4 FEB 2017

Intraslab rupture triggering megathrust rupture coseismically in the 17 December 2016 Solomon Islands M_w 7.9 earthquake

Thorne Lay[1], Lingling Ye[2], Charles J. Ammon[3], and Hiroo Kanamori[2]

[1]Department of Earth and Planetary Sciences, University of California, Santa Cruz, California, USA, [2]Seismological Laboratory, California Institute of Technology, Pasadena, California, USA, [3]Department of Geosciences, Pennsylvania State University, University Park, Pennsylvania, USA

Abstract The 17 December 2016 Solomon Islands earthquake (M_w 7.9) initiated ~103 km deep in the subducting Solomon Sea slab near the junction of the Solomon Islands and New Britain trenches. Most aftershocks are located near the Solomon Islands plate boundary megathrust west of Bougainville, where previous large interplate thrust faulting earthquakes occurred in 1995 (M_w 7.7) and 1971 (M_w 8.0). Teleseismic body wave modeling and aftershock relocations indicate that the initial 30 s of the 2016 rupture occurred over depths of 90 to 120 km on an intraslab fault dipping ~30° to the southwest, almost perpendicular to the dipping slab interface. The next 50 s of rupture took place at depths of 32 to 47 km in the deeper (Domain C) portion of the overlying megathrust fault dipping ~35° to the northeast. High susceptibility to triggering in the region accounts for this compound rupture of two separate fault planes.

1. Introduction

Some very large earthquakes involve faulting on distinct fault planes. The faulting can trigger coseismically in a compound event, or have delayed triggering, resulting in isolated doublet or triplet sequences. Coseismic triggering can only be quantified by detailed analysis of the interfering waveforms. The 29 September 2009 Samoa M_w 8.1 outer rise normal faulting earthquake triggered coseismic M_w 8.0 interplate thrust faulting in the Tonga subduction zone [e.g., *Beavan et al.,* 2010; *Lay et al.,* 2010; *Fan et al.,* 2016]. The 4 June 2000 Enganno (Sumatra) M_w 7.9 intraslab strike-slip faulting event triggered coseismic interplate thrust faulting [e.g., *Abercrombie et al.,* 2003]. The 11 April 2012 Indo-Australian M_w 8.7 rupture involved coseismic rupture of at least four near-orthogonal strike-slip faults [e.g., *Yue et al.,* 2012; *Wei et al.,* 2013; *Hill et al.,* 2016]. The 7 December 2012 Japan M_w 7.2 near-trench intraslab compressional earthquake immediately triggered an M_w 7.1 outer rise normal faulting [*Lay et al.,* 2013]. The 15 November 2006 Kuril M_w 8.3 interplate thrust faulting earthquake immediately activated outer rise faulting that culminated in the 13 January 2007 M_w 8.1 outer rise normal faulting earthquake [e.g., *Ammon et al.,* 2008; *Lay et al.,* 2009]. These, among other examples, indicate near-critical stress conditions on regional faults that can be driven to failure by static and/or dynamic stress changes from nearby large ruptures [e.g., *Christensen and Ruff*, 1988; *Lay et al.,* 1989].

Large earthquake doublets and triplets of comparable size events have long been recognized to be common in certain regions, notably the Solomon Islands-New Britain subduction zone [*Lay and Kanamori*, 1980; *Schwartz et al.,* 1989; *Xu and Schwartz*, 1993; *Furlong et al.,* 2009]. Any given instance of a large earthquake doublet can certainly be viewed as a low probability occurrence of an aftershock comparable to or exceeding an initial event's magnitude [e.g., *Felzer et al.,* 2004]. Where there is a regional tendency for such sequences to be more common than elsewhere the behavior is usually associated with generally higher regional levels of aftershock productivity [*Felzer et al.,* 2004; *Wetzler et al.,* 2016] and/or by specific attributes of regional stress heterogeneity that favor large event triggering interactions [e.g., *Lay and Kanamori*, 1981].

On 17 December 2016 a major earthquake [*U.S. Geological Survey, National Earthquake Information Center* (USGS-NEIC; http://earthquake.usgs.gov/earthquakes/eventpage/us200081v8#executive) 10:51:12.57 UTC, 4.509°S, 153.450°E, 103.2 km deep] struck near the junction of the Solomon Islands and New Britain trenches (Figure 1). The rapid global centroid moment tensor (GCMT; http://www.globalcmt.org/CMTsearch.html) solution has a centroid location at 5.56°S, 153.83°E, 53.3 km deep (Figure 2), a centroid time of 42.1 s, and a seismic moment $M_0 = 8.4 \times 10^{20}$ Nm. It is almost a pure double-couple solution with possible fault plane orientations given by strike, $\varphi_1 = 141°$, dip, $\delta_1 = 36°$, and rake, $\lambda_1 = 96°$ and $\varphi_2 = 313°$, $\delta_2 = 54°$, and $\lambda_2 = 86°$.

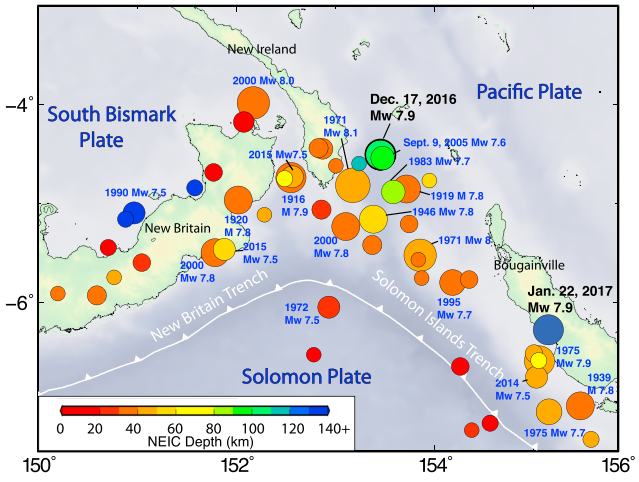

Figure 1. Earthquake epicenters from 1900 to 2016 with magnitude larger than 7 from the USGS-NEIC catalog for the region near the junction of the New Britain and Solomon Islands trenches. Each event circle is scaled proportional to magnitude and color coded for hypocentral depth. Events with magnitudes larger than 7.5 are labeled in blue.

The hypocenter is consistent with the source initiating within the underthrust Solomon Sea slab which drapes around the 90° corner between the two trenches (Figures 1 and S1 in the supporting information). However, the difference between the centroid depth and the hypocentral depth indicates significant vertical extent of the seismic radiation, and the NEIC-USGS rapid finite-fault solution favors rupture extending about 100 km in depth on the more steeply dipping plane. The USGS-NEIC discussion of their solution suggests that triggering of motion along the plate boundary may have been involved. We analyze the teleseismic observations for the 2016 event to determine the source process and interaction between the intraslab and interplate environments. While this paper was in review, a second M_w 7.9 intermediate depth event occurred on 22 January 2017 (04:30:23 UTC, 6.214°S, 155.122°E) with a hypocenter 136 km below Bougainville, southeast from the 2016 event (Figure 1). We determine a *W* phase centroid depth of 140.5 km, and the quick GCMT centroid depth is 146.8 km. The 2017 earthquake can be viewed as the second event in a large intermediate earthquake doublet, but it does not appear to involve a large depth extent of rupture like the 2016 event.

2. Analysis of the Source Process

To further constrain the long-period point-source parameters, we performed long-period *W* phase inversions for the 17 December 2016 Solomon Islands event using 2 to 5 MHz ground motions on 97 channels recorded at 45 stations. The centroid depth is estimated as 60.5 km, with a 40 s centroid time, and the moment tensor is predominantly double couple with fault plane orientations given by $\varphi_1 = 138°$, $\delta_1 = 42°$, and $\lambda_1 = 86°$ and $\varphi_2 = 323°$, $\delta_2 = 48°$, and $\lambda_2 = 93°$, with a seismic moment of 8.8×10^{20} Nm (M_w 7.9). This final solution is representative of solutions for which the inversion initiated at different depths and in which we used up to 655 channels, and it supports the finding that the rupture must have significant vertical extent.

In order to determine the spatial extent of the rupture, we use a linear least squares kinematic finite-fault inversion of teleseismic body waves [e.g., *Hartzell and Heaton*, 1983; *Kikuchi and Kanamori*, 1992; *Ye et al.,* 2016a]. We invert 130 s long windows of 68 *P* wave displacements and *35 SH* wave ground velocities (which have dominant periods similar to the *P* wave displacements) filtered in the frequency range 0.005 to 1.0 Hz. Given the almost pure double-couple solutions provided by the long-period GCMT and *W* phase inversions, we initially considered ruptures on single fault planes from the best double-couple faulting geometries. Rupture on the more steeply dipping plane is preferred, as the solutions place significant slip on the shallow portion of the fault planes. A finite-fault inversion using the 54° dipping plane of the GCMT solution is shown in Figure S2, with slip exceeding 1 m distributed from 60 to 130 km and in the uppermost 20 km. The slip centroid depth is 52 km, and the centroid time is 41.6 s, consistent with the GCMT values. For all models shown here, the subfault source time functions are parameterized by 6 2.5 s rise time symmetric triangles lagged in onset by 2.5 s each, for total possible subfault durations of 17.5 s. The slip distribution is generally similar to the USGS-NEIC solution for a single planar fault, although our model places the shallow slip farther to the southeast along the Solomon Islands trench. The M_0 estimate is 8.8×10^{20} Nm. The planar model provides acceptable waveform matches but is very difficult to interpret, as the 54° dip is comparable to the dip of the slab at intermediate depths, based on model Slab 1.0 [*Hayes et al.,* 2012]. The upward extrapolation of this fault cuts into the upper wedge of the subduction zone if it extends to the shallow depths favored by the

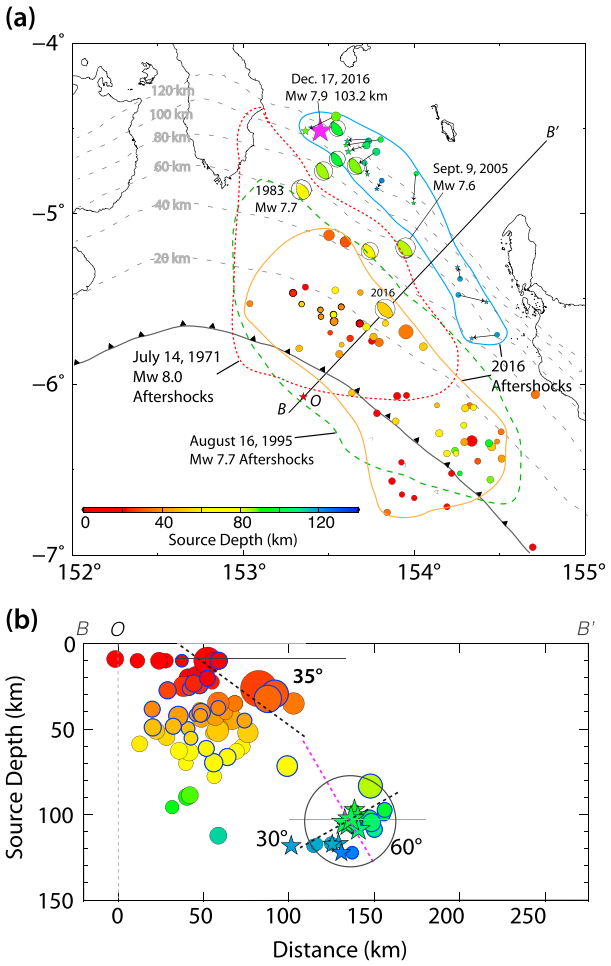

Figure 2. (a) Comparison of 1 week USGS/NEIC aftershock distributions for the 17 December 2016 M_w 7.9 event (intermediate depth events outlined in blue, shallow events in orange), the 16 August 1995 M_w 7.7 interplate earthquake (outlined by the dashed green line), and the 14 July 1971 M_w 8.0 interplate earthquake (outlined by the dotted red curve) [*Lay and Kanamori*, 1980]. Depth contours for Slab 1.0 are shown by gray dashed lines. The intraslab aftershocks were relocated relative to the main shock, with the arrow pointing from the NEIC to the relocated positions (stars). The magenta star indicates the NEIC epicenter. The GCMT mechanism for the 2016 event is plotted at the centroid location. GCMT focal mechanisms for events with $M_w \geq 6.0$ from 1976 to 2016 for the depth range 60 to 130 km are also shown. Note the similarity of mechanisms of the latter events. The largest intermediate depth event prior to 2016 is an M_w 7.7 event in 1983 at a depth of 70 km with a centroid location southwest of the 2016 epicenter. (b) Vertical cross section along azimuth N43°E through the aftershock distribution along the line B-B′ in Figure 2a. The blacked dashed lines indicate the rupture plane geometry for the model in Figure 3. The magenta dashed line is the alternate 60° dipping deep fault model shown in Figure S7.

inversion. There is no clear basis for assuming that the plate boundary is seismogenic from 60 to 130 km depth, so an intraplate rupture paralleling the deeper plate surface must be invoked for this scenario.

Figure 2 clearly raises the possibility of a change in faulting orientation with depth. Note that the first week of aftershock locations for the 2016 event has two clusters of aftershock depths, from 90 to 118 km and shallower than 50 km, consistent with two slip patches at different depths. The deeper aftershocks were relocated in horizontal position relative to the main shock, tightening their along-strike alignment (stars). Figure S3 shows the relationship of the aftershocks to the background seismicity. The shallow aftershock distribution has surprising similarity to the aftershock sequences of the two large underthrusting ruptures of the Solomon Islands megathrust on 16 August 1995 (M_w 7.7) [*Ye et al.*, 2016a] and 14 July 1971 (M_w 8.0) [*Lay and Kanamori*, 1980], indicating activation of the shallow fault by the deep intraslab faulting. The routine short-period *P* wave backprojections produced by the Incorporated Research Institutions for Seismology for this event [http://ds.iris.edu/spud/backprojection/13341772] indicate significant radiation to the southeast of the hypocenter, near the shallow aftershock locations. Thus, rather than extending the rupture plane along constant dip, we explored rupture models with varying dip, using the shallow geometry of Slab 1.0 as a guide on the megathrust geometry and specifying a steeper dip for the intraplate rupture. To constrain the deeper geometry, we considered all GCMT focal mechanisms since 1976 for M_w 6.0–7.7 events in the depth range 60 to 130 km near the 2016 rupture zone. The event with NEIC hypocenter closest to the hypocenter is that of 9 September 2005, M_w 7.6. Figure 2 shows that there is similarity in many of the mechanisms, which have an average steeper dip of 60° and shallower dip of 30°, the same as the 2005 event. We fix these as options for the deep faulting geometry, noting that as long as the strike and pure dip-slip rake of the deep and shallow faulting are the same, the overall moment tensor for a dip-varying model will be close to a pure double couple as required by the long-period inversions.

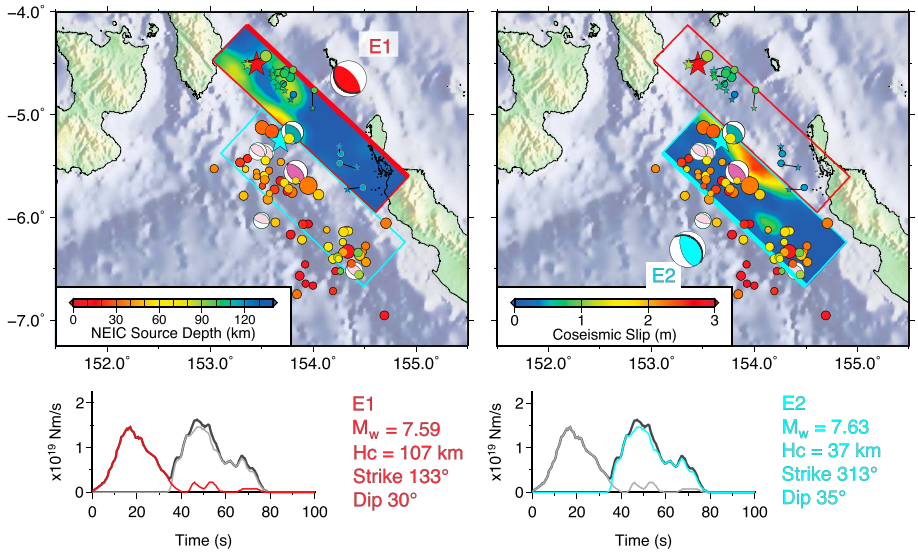

Figure 3. The preferred two-fault rupture model for the 17 December 2016 M_w 7.9 Solomon Islands earthquake. The first fault to rupture is labeled E1, with the map view of the fault position (shallower edge is heavier line, red star is the hypocenter) and the slip distribution shown on the top left, and the moment rate function in red below. The second fault to rupture is labeled E2, with the map view of the fault position (shallower edge is heavier line, cyan star is the hypocenter) and the slip distribution shown on the top right, and the moment rate function in cyan below. The total moment rate function is shown by the black trace. The faulting geometry for E1 is shown by the red focal mechanism and the faulting geometry for E2 is shown by the cyan focal mechanism (fault planes are indicated by heavier black lines), with the respective faulting parameters (Hc is slip centroid depth) shown below. The 1 week aftershocks from the USGS-NEIC are shown by circles with color-coded depths and size scaled proportional to magnitude. The relocated intermediate depth event hypocenters are shown by small stars. The magenta focal mechanism is the GCMT solution plotted at the centroid location. The forest green focal mechanism is the composite focal mechanism of the two-faulting slip model at the faulting centroid. Pink focal mechanisms are GCMT solutions for larger aftershocks.

We next considered a continuous rupture on a dip-varying rupture surface extending from the trench with dip increasing from 10° to 35° at a depth of 50 km and then along a 60° dipping fault down to the hypocenter (Figure S4). A rupture velocity of 3.0 km/s is used in the case shown, but this is not uniquely constrained. Two slip patches are found at depths from 70 to 133 km and from 30 to 50 km. The latter patch occurs just above the shallowing of the fault dip, indicating that the more realistic shallow dip of the megathrust geometry favors slip on the deeper portion of the megathrust rather than up to the near surface. This model of continuous rupture expansion over the dip-varying geometry accounts for 85% of the waveform power and is the most successful model in terms of fitting the waveforms of all that we considered.

Despite the good waveform fit achieved for the single dip-varying fault model, there are several reasons to question such a model. Smooth expansion of rupture from the intraslab environment to the megathrust environment may be plausible, but it is not clear that the faults connect uniformly. The 60° dipping fault in the slab does not have aftershocks along its entire depth extent, and as apparent in Figure 2, the intermediate depth aftershocks actually are deeper toward the southwest from the hypocenter, conflicting with the steep fault geometry. Also, as apparent in Figures 1 and S1, the shallow megathrust curves around the bend to the New Britain trench geometry updip of the hypocenter, so planar connected surfaces are not realistic. Thus, we explore two discrete fault models, one involving an intraslab fault dipping at 30° toward the southwest (accounting for the deepening of the aftershocks to depths of 118 km) and the other a 35° dipping shallow fault corresponding to the geometry of the deeper portion of the Solomon Island megathrust, with the fault translated 75 km southeastward away from the trench junction on the plate boundary.

Figure 3 shows the two-fault slip model for a rupture velocity of 3.0 km/s on both faults, with the hypocenter of the shallow fault (cyan star) being 40 km deep, and rupture initiating 30 s after the deep hypocenter. The strike of the deep fault is 313° (red mechanism) and that of the shallow fault is 133° (cyan mechanism), so the composite moment tensor (green mechanism) is close to a pure thrust double couple, and similar to the GCMT solution (pink mechanism). The along-dip extent of both faults is delimited to constrain slip to reasonable seismogenic portions of the megathrust and the intraslab environment. Slip in the deeper fault

ranges up to 2 m, while that in the shallow fault ranges up to 2.4 m (Figure S5). The two-fault model fits the observed waveform data (Figure S6) about the same as the single-fault model using the GCMT geometry (75% of the waveform power is accounted for), but not as well as the changing-dip continuous rupture. This is largely due to the greater degrees of freedom of the continuous rupture model as it reaches the shallow portion of the fault over an extended rupture front that allows a broad range of subfaults to activate. In contrast, the two-fault model initiates the shallow rupture from a single subfault. A similar two-fault model with the deep fault dip being 60° (Figure S7) gives a comparable waveform fit.

We determined a range of two fault models with different rupture velocities, fault placement, triggering time and location, and subfault durations. The model in Figure 3 is certainly not uniquely resolved, but it is a solution consistent with what is known or most reasonable for the event. Slip is relatively large at the deeper edge of both faults, but we do not extend the models deeper because doing so leads to an unreasonable extent of slip on the megathrust or within the slab. The distribution of intermediate depth aftershocks is well accounted for by the 30° dip, deepening toward the southwest (Figures 2 and 3). This places the deep fault plane nearly perpendicular to the slab dip, compatible with a reactivated fracture zone in the Solomon Sea slab. We consider that much more likely than a slab dip-parallel intraslab rupture or frictional sliding of the slab interface, as implied by the 60° dip option, which also does not fit the aftershock pattern. The shallow rupture locates on the deeper portion of the megathrust (Domain C in the model of *Lay et al.* [2012]), which is compatible with a moderately high rupture velocity of 3.0 km/s for the shallow rupture. The overall moment tensor for the finite fault model is similar to the long-period solutions, although the centroid depth is about 13 km deeper than the GCMT and *W* phase results. The first 35 s of rupture is entirely on the deep fault and has a moment of 3.0×10^{20} Nm (M_w 7.6), and the next 50 s of rupture is predominantly on the shallow fault and has a moment of 3.5×10^{20} Nm (M_w 7.6). While we cannot absolutely preclude rupture on the steeper dip plane for the intraslab rupture, we consider the model in Figure 3 to be more realistic.

3. Earthquake Susceptibility to Triggering

Intraslab rupture has been found to trigger faulting on the megathrust for several large earthquakes, but the 17 December 2016 Solomon Islands event appears to be a rare case of intermediate depth rupture triggering megathrust rupture coseismically. If there is any region that such triggering might be expected, it is the Solomon Islands, which tends to produce strong interactions between large events. In this regard, the 2016 event can be viewed as a doublet rupture of distinct fault planes that fail coseismically. This is similar to the 2009 Samoa earthquake doublet, in which an outer rise rupture triggered the megathrust about 50 km away. Here the distance between the fault planes is comparable, about 60 km. The time sequence of USGS-NEIC seismicity in the New Britain-Solomon Islands subduction zones (Figures 1 and S8) indicates very intense activity near the trench junction and occurrence of large earthquake doublets in 1971, 1974, 1975, 2000, and 2015, all close to the 2016 source region. Even the 1 April 2007 M_w 8.1 rupture can be viewed as a doublet, as it ruptured two large slip patches on different plates across a triple junction [*Furlong et al.,* 2009]. The region has a high background seismicity rate and high aftershock productivity [*Felzer et al.,* 2004], which accounts for high susceptibility to triggering in general. In conjunction with the spacing of the modest-size strongly coupled portions (asperities) of the New Britain and Solomon Islands megathrusts, the tendency for large doublet occurrence is heightened locally.

On 9 September 2005, an M_w 7.6 intraslab earthquake struck near 94 km depth very close to the 2016 hypocenter (Figure 1), with a GCMT centroid not far from the 2016 solution (Figure 2). The 2005 event has the same faulting geometry as assumed for the deep rupture in 2016, and about the same seismic moment. The first week aftershock sequence is more productive but otherwise spans a similar horizontal extent to the deep part of the aftershock pattern for 2016. Deeper aftershocks again locate on the southwest side of the distribution, and a 30° dipping trend about 30 km deeper than that in Figure 2 suggests rupture of a parallel plane (Figure S9). However, the 2005 event triggered only a few aftershocks near the megathrust. We performed finite-fault inversions for the 2005 event and did not find clear preference for the 60° or 30° dipping planes, as is the case for the USGS-NEIC finite fault solution. The 22 January 2017 M_w 7.9 intermediate depth event triggered only two shallow aftershocks near the megathrust within the first 2 days, far less that what followed the 2016 rupture, indicating that the critically stressed regions had largely been released by the first member of the doublet.

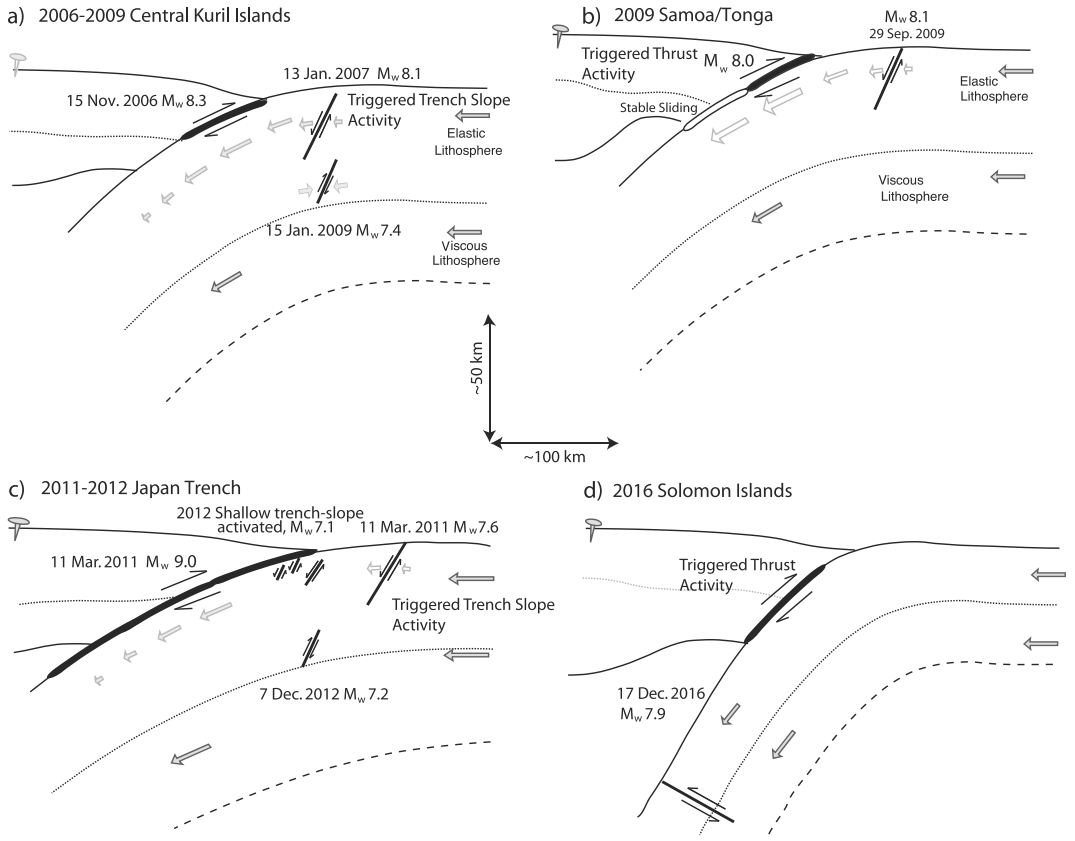

Figure 4. Schematic displays of large earthquake triggering sequences involving distinct faults that fail either (b, d) coseismically or (a, c) with delays of hours to months. Open arrows indicate the coseismic sense of motion in the slab for each event, with shaded arrows indicating long-term motion that loads the elastic system and drives the viscous system. The 15 November 2006 M_w 8.3 interplate thrust in the Kuril subduction zone activated outer trench normal faulting immediately and 60 days later an M_w 8.1 normal faulting earthquake occurred (Figure 4a). Trench slope normal faulting in northern Tonga occurred on 29 September 2009 (M_w 8.1) and triggered coseismic thrust faulting on the megathrust (M_w 8.0) (Figure 4b). The 11 March 2011 M_w 9.0 interplate thrust triggered extensive trench slope and outer rise normal faulting including an M_w 7.6 event about 30 min after the main shock (Figure 4c). The 2016 Solomon Islands M_w 7.9 earthquake initiated with intraplate rupture on a shallow dipping plane about 100 km deep and triggered coseismic interplate thrusting with comparable moment (Figure 4d).

Triggering of a M_w ~7.6 megathrust rupture 21 years after the last large event in 1995 is not extraordinary given the relatively short recurrence time of ~25 years observed for historic large earthquakes in the Solomon Islands [e.g., *Lay and Kanamori*, 1980] and the 24 year interval between the preceding 1971 and 1995 ruptures of the same region. The precise location of the slip has uncertainty, and it is not possible for us to resolve whether the same large-slip areas reruptured.

4. Discussion and Conclusions

Several observed scenarios for large earthquake triggering interactions involving distinct fault planes in subduction zones are depicted in Figure 4. The 2016 Solomon Islands event is the first instance of well-documented triggering of large megathrust rupture coseismically by downdip intraslab thrust faulting, although relatively deep outer rise compressional events have been observed to activate both shallow normal faulting and minor interplate seismicity [e.g., *Ye et al.*, 2012; *Todd and Lay*, 2013]. It is important to recognize that the similarity in strike and rake of the two subevents in the 2016 rupture causes the combined radiation to be compatible with an intermediate geometry almost pure double couple. Detecting such faulting complexity requires detailed investigation, and prior instances of similar triggering may have been missed.

The efficacy of triggering by the static and dynamic stresses from the first large event in each scenario indicates that adjacent fault systems are near their critical failure stresses. For the 2016 Solomon Islands event, this is due to the buildup of strain around the megathrust since the 1995 M_w 7.7 earthquake. The 2005 event failed to drive failure of the megathrust despite having similar location and size to the 2016 event. It appears that the additional 11 years of stress accumulation pushed the megathrust close enough to critical failure stress levels that it could be triggered in the recent event. The seismic hazard posed by intermediate earthquake faulting near 100 km depth has received increasing attention [e.g., *Ye et al.,* 2016b], but the potential for coseismic triggering of a large shallow megathrust rupture adds an additional hazard that needs to be considered for regions that have approached their critical failure state.

Acknowledgments
The IRIS DMS data center (http://www.iris.edu/hq/) was used to access the seismic data from Global Seismic Network and Federation of Digital Seismic Network stations. We thank Chen Ji and an anonymous reviewer for constructive reviews of the manuscript. This work was supported by U.S. NSF grant EAR1245717 to Thorne Lay.

References

Abercrombie, R. E., M. Antolik, and G. Ekström (2003), The June 2000 M_w 7.9 earthquakes south of Sumatra: Deformation in the India-Australia Plate, *J. Geophys. Res.*, *108*(B12018), ESE 6-1–ESE 6-16, doi:10.1029/2001JB000674.

Ammon, C. J., H. Kanamori, and T. Lay (2008), A great earthquake doublet and seismic stress transfer cycle in the central Kuril Islands, *Nature*, *451*, 561–565, doi:10.1038/nature06521.

Beavan, J., X. Wang, C. Holden, K. Wilson, W. Power, G. Prasetya, M. Bevis, and R. Kautoke (2010), Near-simultaneous great earthquakes at Tongan megathrust and outer rise in September 2009, *Nature*, *466*, 959–963, doi:10.1038/nature09292.

Christensen, D. H., and L. J. Ruff (1988), Seismic coupling and outer rise earthquakes, *J. Geophys. Res.*, *93*(B11), 13,421–13,444, doi:10.1029/JB093iB11p13421.

Fan, W., P. M. Shearer, C. Ji, and D. Bassett (2016), Multiple branching rupture of the 2009 Tonga-Samoa earthquake, *J. Geophys. Res. Solid Earth*, *121*, 5809–5827, doi:10.1002/2016JB012945.

Felzer, K. R., R. E. Abercrombie, and G. Ekström (2004), A common origin for aftershocks, foreshocks and multiplets, *Bull. Seism. Soc. Am.*, *94*, 88–98.

Furlong, K. P., T. Lay, and C. J. Ammon (2009), A great earthquake rupture across a rapidly evolving three-plate boundary, *Science*, *324*, 226–229.

Hartzell, S. H., and T. H. Heaton (1983), Inversion of strong ground motion and teleseismic waveform data for the fault rupture history of the 1979 Imperial Valley, California, earthquake, *Bull. Seismol. Soc. Am.*, *73*(6A), 1553–1583.

Hayes, G. P., D. J. Wald, and R. L. Johnson (2012), Slab 1.0: A three-dimensional model of global subduction zone geometries, *J. Geophys. Res.*, *117*, B01302, doi:10.1029/2011JB008524.

Hill, E. M., et al. (2016), The 2012 M_w 8.6 Wharton Basin sequence: A cascade of great earthquakes generated by near-orthogonal, young, oceanic mantle faults, *J. Geophys. Res. Solid Earth*, *120*, 3723–3747, doi:10.1002/2014JB011703.

Kikuchi, M., and H. Kanamori (1992), Inversion of complex body waves—III, *Bull. Seismol. Soc. Am.*, *81*(6), 2335–2350.

Lay, T., and H. Kanamori (1980), Earthquake doublets in the Solomon Islands, *Phys. Earth and Planet. Inter.*, *21*, 283–304.

Lay, T., and H. Kanamori (1981), An asperity model of large earthquake sequences, in *Earthquake Prediction*, *an International Review*, *Maurice Ewing Series*, *IV*, 579–592, edited by D. W. Simpson and P. G. Richards, AGU, Washington, D. C.

Lay, T., L. Astiz, H. Kanamori, and D. H. Christensen (1989), Temporal variation of large intraplate earthquakes in coupled subduction zones, *Phys. Earth Planet. Inter.*, *54*, 258–312.

Lay, T., H. Kanamori, C. J. Ammon, A. R. Hutko, K. Furlong, and L. Rivera (2009), The 2006–2007 Kuril Islands great earthquake sequence, *J. Geophys. Res.*, *114*, B113208, doi:10.1029/2008JB006280.

Lay, T., C. J. Ammon, H. Kanamori, L. Rivera, K. D. Koper, and A. R. Hutko (2010), The 2009 Samoa-Tonga great earthquake triggered doublet, *Nature*, *466*, 964–968, doi:10.1038/nature09214.

Lay, T., H. Kanamori, C. J. Ammon, K. D. Koper, A. R. Hutko, L. Ye, H. Yue, and T. M. Rushing (2012), Depth-varying rupture properties of subduction zone megathrust faults, *J. Geophys. Res.*, *117*, B04311, doi:10.1029/2011JB009133.

Lay, T., Z. Duputel, L. Ye, and H. Kanamori (2013), The December 7, 2012 Japan Trench intraplate doublet (M_w 7.2, 7.1) and interactions between near-trench intraplate thrust and normal faulting, *Phys. Earth Planet. Inter.*, *220*, 73–78, doi:10.1016/j.pepi.2013.04.009.

Schwartz, S. Y., T. Lay, and L. J. Ruff (1989), Source process of the great 1971 Solomon Islands doublet, *Phys. Earth Planet. Inter.*, *56*, 294–310.

Todd, E. K., and T. Lay (2013), The 2011 Northern Kermadec earthquake doublet and subduction zone faulting interactions, *J. Geophys. Res. Solid Earth*, *118*, 1–13, doi:10.1029/2012JB009711.

Wei, S., D. Helmberger, and J.-P. Avouac (2013), Modeling the 2012 Wharton basin earthquakes off-Sumatra: Complete lithospheric failure, *J. Geophys. Res. Solid Earth*, *118*, 3592–3609, doi:10.1002/jgrb.50267.

Wetzler, N., E. Brodsky, and T. Lay (2016), Aftershock productivity of large megathrust earthquakes: Regional variations and influence of mainshock source parameters, *Geophys. Res. Lett.*, *43*, doi:10.1002/2016GL071104.

Xu, Z., and S. Y. Schwartz (1993), Large earthquake doublets and fault plane heterogeneity in the northern Solomon Islands subduction zone, *Pure Appl. Geophys.*, *140*, 365–390.

Ye, L., T. Lay, and H. Kanamori (2012), Intraplate and interplate faulting interactions during the August 31, 2012 Philippine Trench earthquake (M_w 7.6) sequence, *Geophys. Res. Lett.*, *39*, L24310, doi:10.1029/2012GL054164.

Ye, L., T. Lay, H. Kanamori, and L. Rivera (2016a), Rupture characteristics of major and great ($M_w \geq 7.0$) megathrust earthquakes from 1990 to 2015: 1. Source parameter scaling relationships, *J. Geophys. Res. Solid Earth*, *121*, 826–844, doi:10.1002/2015JB012426.

Ye, L., T. Lay, H. Kanamori, J. T. Freymueller, and L. Rivera (2016b), Joint inversion of high-rate GPS and teleseismic observations for rupture process of the 23 June 2014 (M_w 7.9) Rat Islands archipelago, Alaska, intermediate depth earthquake, in *Plate Boundaries and Natural Hazards*, edited by J. C. Duarte and W. P. Schellart, pp. 149–166, American Geophysical Union Monograph 219.

Yue, H., T. Lay, and K. D. Koper (2012), En échelon and orthogonal fault ruptures of the 11 April 2012 great intraplate earthquakes, *Nature*, *490*, 245–249 doi:10.1038/nature11492.

Geophysical Research Letters

Supporting Information for

Intraslab rupture triggering megathrust rupture co-seismically in the December 17, 2016 Solomon Islands M_w 7.9 earthquake

Thorne Lay[1], Lingling Ye[2], Charles J. Ammon[3], and Hiroo Kanamori[2]

[1]Department of Earth and Planetary Sciences, University of California Santa Cruz, Santa Cruz, California, USA, [2]Seismological Laboratory, California Institute of Technology, Pasadena, California, USA, [3]Department of Geosciences, The Pennsylvania State University, University Park, Pennsylvania, USA, USA

Correspondence to: Thorne Lay, tlay@ucsc.edu

Contents of this file

Figures S1 to S9

Introduction

Supporting information includes 9 figures.

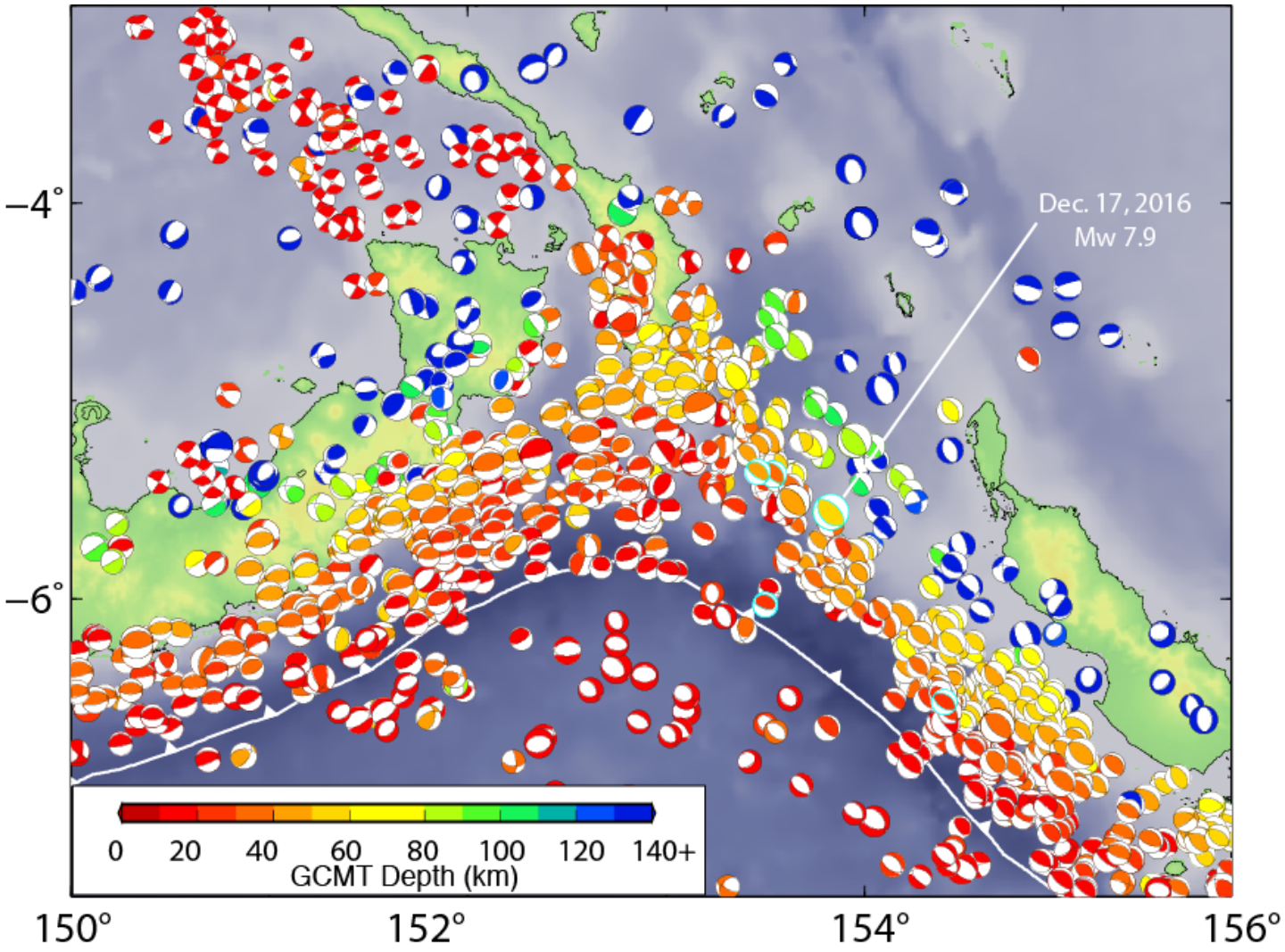

Figure S1. Global centroid moment tensor (GCMT) solutions for all events with $M_W \geq 5.0$ from 1976 to 2016 for the region near the junction of the New Britain and Solomon Islands trenches. The lower hemisphere focal mechanisms are plotted at the centroid locations and color-coded for centroid depth. The radius of each focal mechanism is proportional to M_W. The December 17, 2016 event is highlighted.

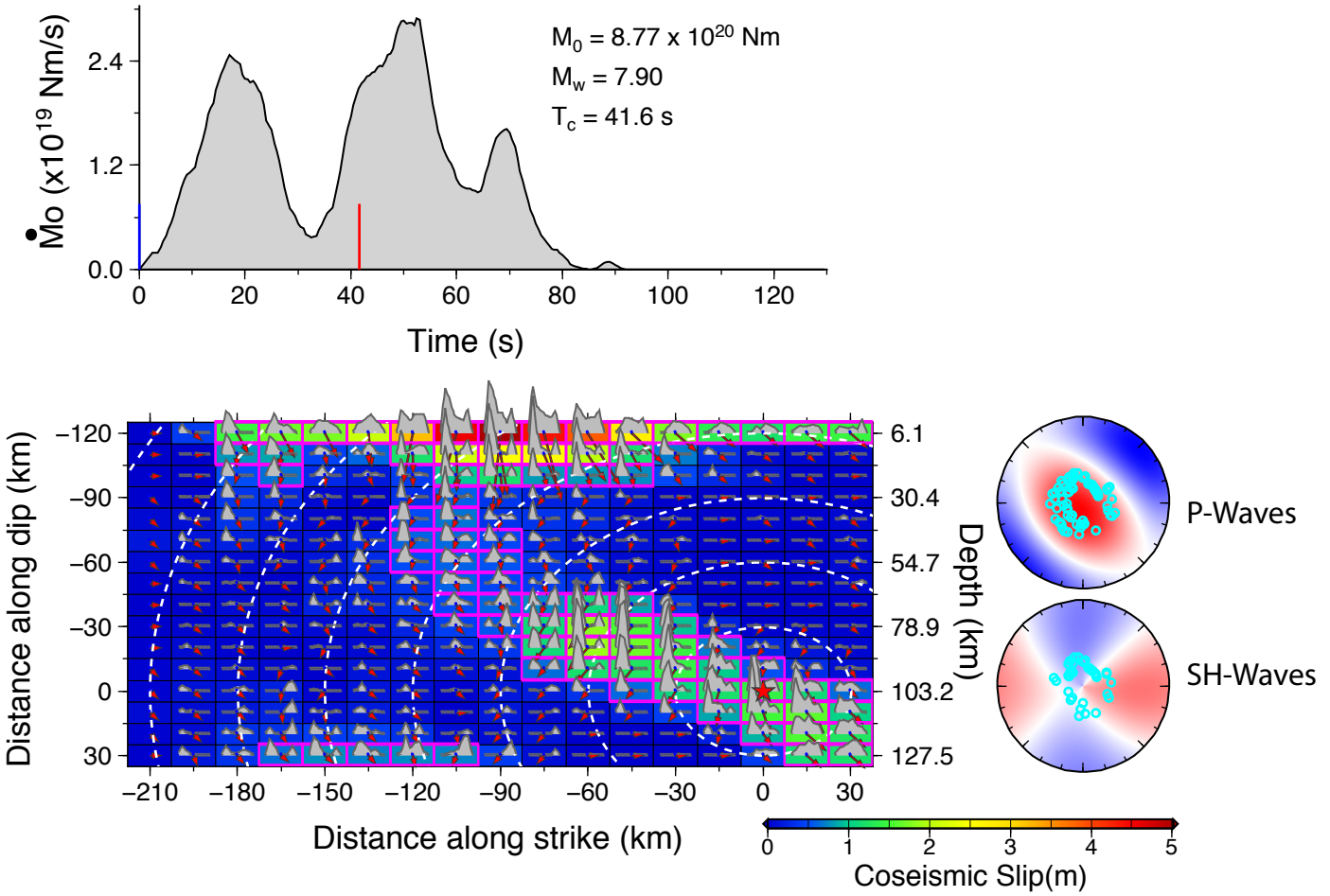

Figure S2. Summary of a planar rupture model that assumes the GCMT best double couple strike (313°) and dip (54°). A rupture velocity of 3 km/s is assumed and the subfaults have 6 2.5-s rise time triangles shifted by 2.5-s each, for total possible subfault durations of 17.5 s. The moment rate function is shown at the top left, with the centroid time (red tick) being T_c = 41.6 s. The slip distribution is shown on the bottom left, with the slip of the footwall shown by the red arrows with magnitude of the total slip in each subfault being color coded. The subfault source time functions are shown within each cell. The rupture fronts at 10 s intervals are shown by white dashed lines. The red star is the hypocenter location. The distribution of *P*-waves and *SH*-waves used in the inversion is shown in the lower hemisphere focal mechanism plots with corresponding radiation patterns color-coded. Constant t* values of 0.75 s and 3.0 s are used for *P*-wave and *SH*-wave modeling, respectively.

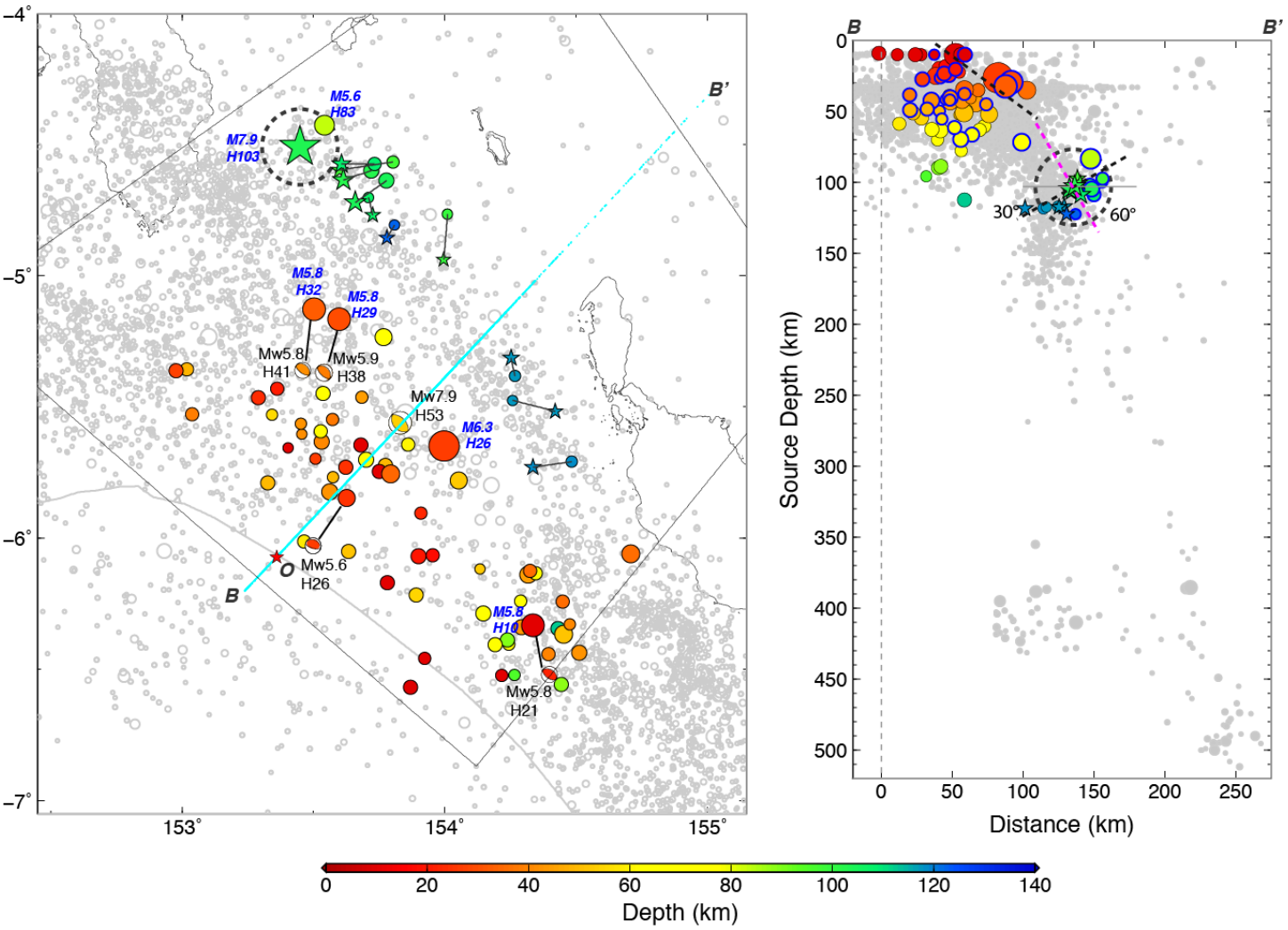

Figure S3. Map view and vertical cross section through the background seismicity (within the black quadrilateral) and the aftershock distribution for the December 17, 2016 Solomon Islands event. USGS-NEIC catalog events with magnitude ≥ 4.5 are shown with small grey circles scaled proportional to magnitude. Aftershocks are shown by circles scaled proportional to magnitude on a larger scale and color-coded with source depth. Large aftershocks are shown at their NEIC locations (with blue labeling of magnitude and hypocentral depth) and with corresponding GCMT mechanisms at the centroid location, (with black labeling of magnitude and centroid depth). Stars indicate the relocated positions of the intermediate depth aftershocks. The large green star surrounded by a dashed circle is the hypocenter of the December 17, 2016 event. In the cross-section, the black-dashed curves indicate the faulting geometries of the two faults in Figure 3, with the magenta curve indicating the dip of the alternate steeply dipping plane for the model in Figure S6. Aftershocks northwest of the reference line B-B′ are outlined in darker black than those to the southeast in the vertical profile.

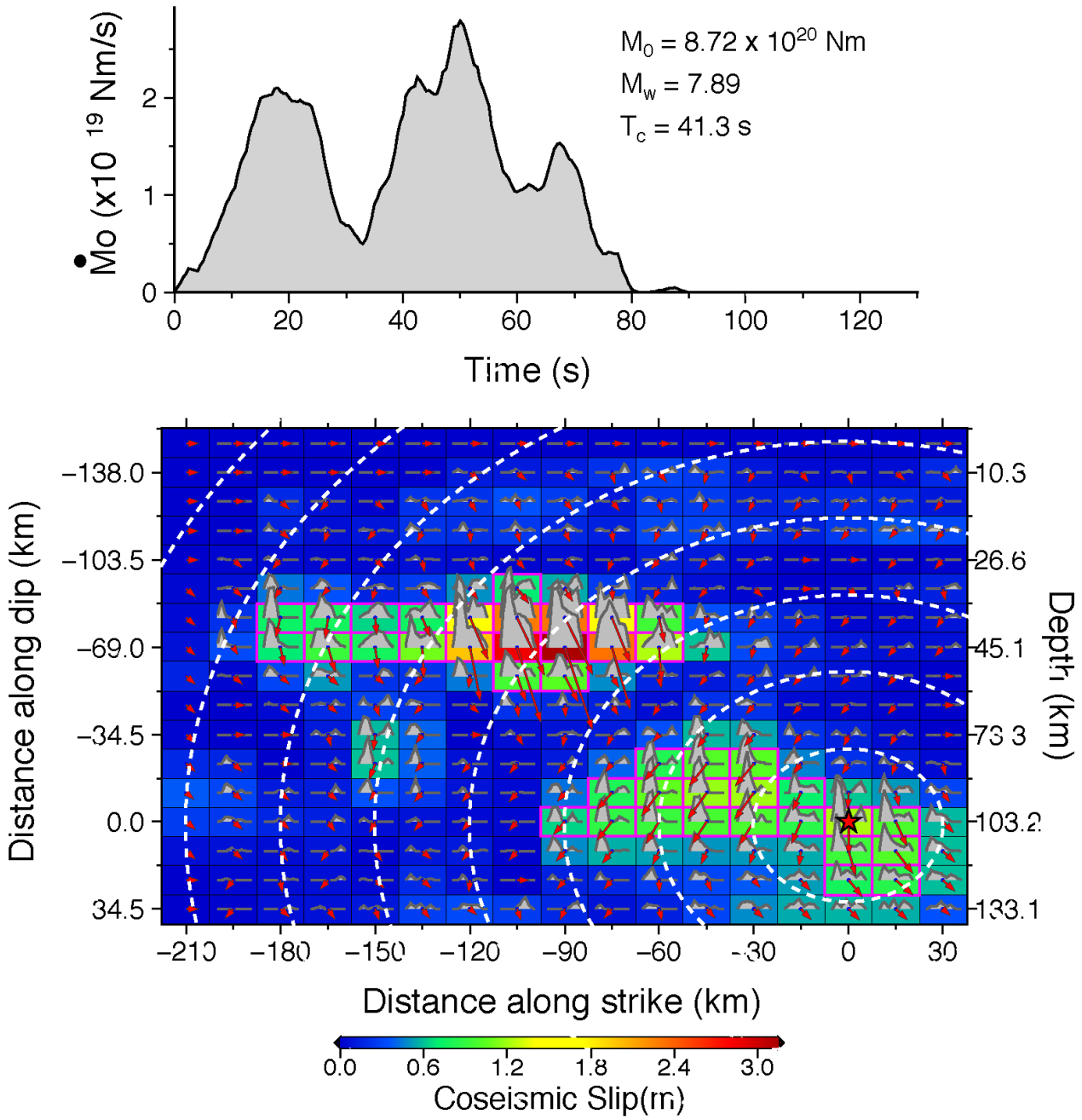

Figure S4. Finite-fault inversion model for a single continuous plane with varying dip ranging from 10° at the up-dip end to 60° below 50 km. The model uses the GCMT best double couple strike (313°). A rupture velocity of 3 km/s is assumed and the subfaults have 6 2.5-s rise time triangles shifted by 2.5-s each, for total possible subfault durations of 17.5 s. The moment rate function is shown at the top, with the centroid time being T_c = 41.3 s. The slip distribution is shown on the bottom, with the slip of the footwall shown by the red arrows with magnitude of the total slip in each subfault being color-coded. The subfault source time functions are shown within each cell. The rupture front at 10 s intervals is shown by white dashed lines. The red star is the hypocenter location. Data sampling is the same as in Figure S2.

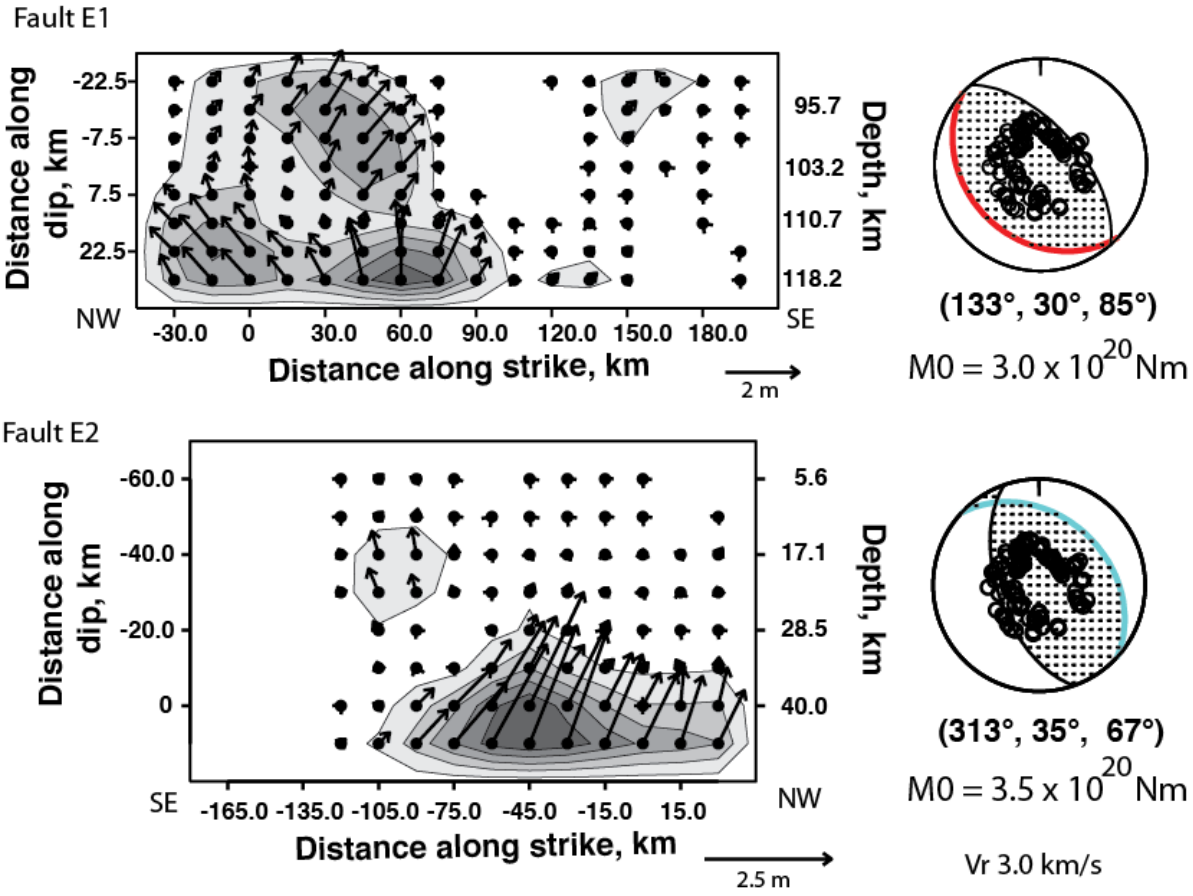

Figure S5. The two-fault finite source rupture model for the December 17, 2016 Solomon Islands earthquake. Fault E1 (shown in map view in Figure 3) is the first fault to fail, with rupture nucleating at 103.2 km depth on a fault dipping 30° toward the SW. The rupture expands at 3.0 km/s, and the first 35 s of the moment rate function in Figure 3 is from slip on E1. Fault E2 (shown in map view in Figure 3) is the second fault to fail, with rupture nucleating at 40 km depth on a fault dipping 35° toward the NE. The last 50 s of the moment rate function is dominated by energy release from Fault E2.

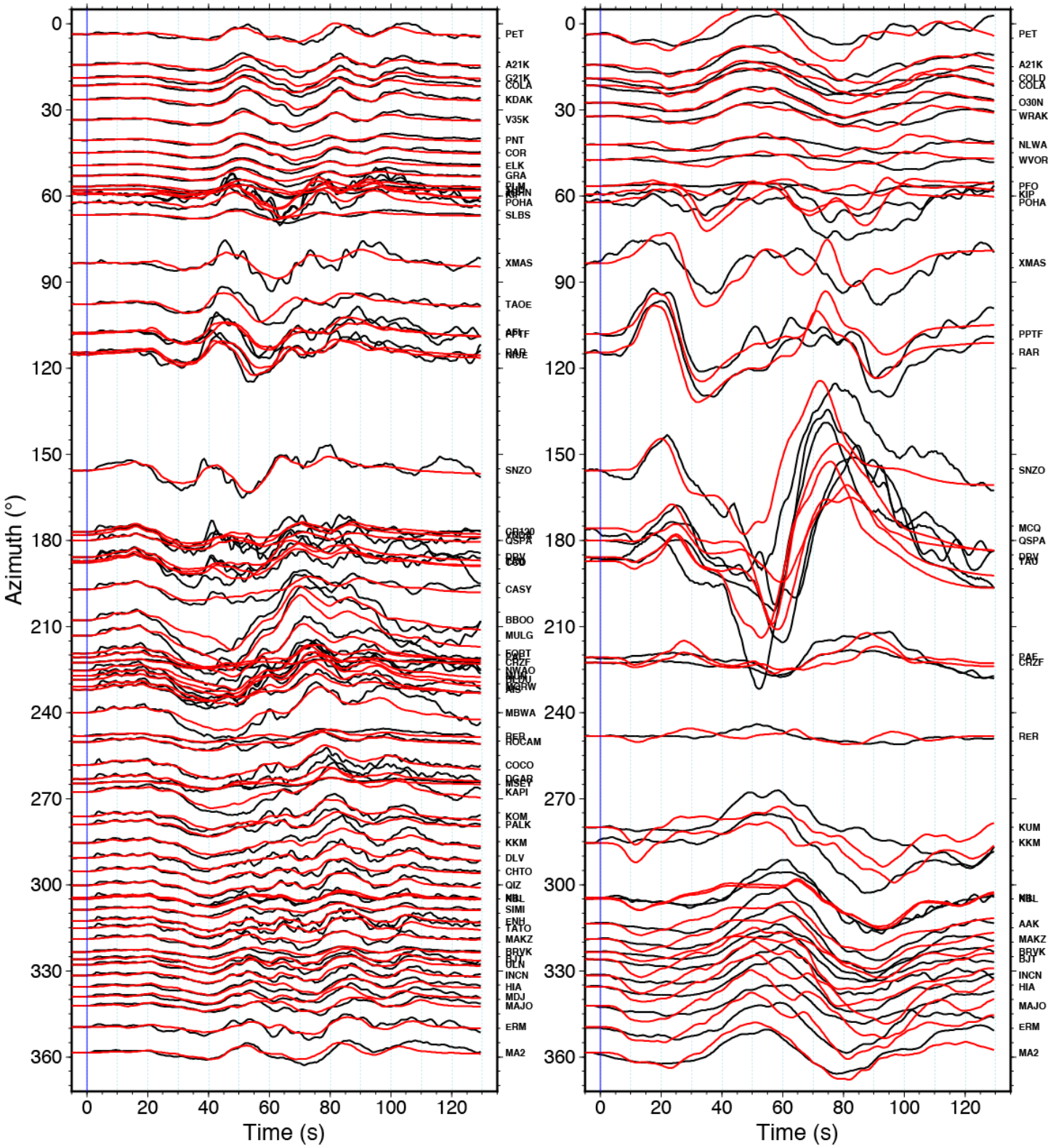

Figure S6. Comparison of observed (black) and computed (red) *P*-wave ground displacements (left panel) and *SH*-wave ground velocities (right panel) for the preferred two-fault rupture model for the December 17, 2016 M_W 7.9 Solomon Islands earthquake shown in Figure 3.

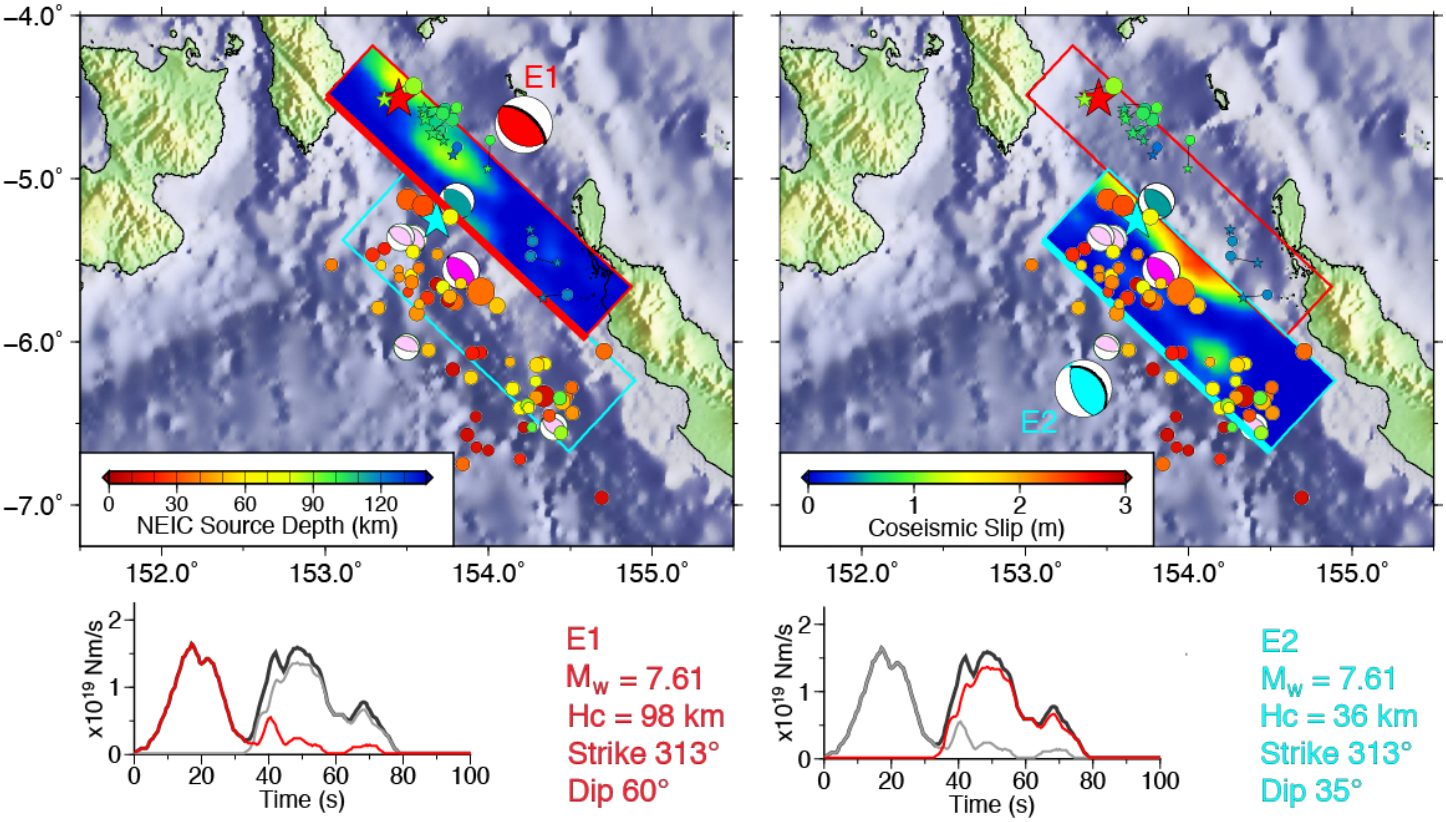

Figure S7. A two-fault rupture model for the December 17, 2016 M_W 7.9 Solomon Islands earthquake using the steeper dipping deep plane as an alternative to the shallow dipping plane used in Figure 3. The first fault to rupture is labeled E1, with the map view of the fault position (shallower edge is heavier line, red star is the hypocenter) and the slip distribution shown on the top left, and the moment rate function in red below. The second fault to rupture is labeled E2, with the map view of the fault position (shallower edge is heavier line, cyan star is the hypocenter) and the slip distribution shown on the top right, and the moment rate function in cyan below. The total moment rate function is shown by the black trace. The faulting geometry for E1 is shown by the red focal mechanism and the faulting geometry for E2 is shown by the cyan focal mechanism (fault planes are indicated by black lines), with the respective faulting parameters (Hc is slip centroid depth) shown below. The one-week aftershocks from the USGS-NEIC are shown by circles with color-coded depths and size scaled proportional to magnitude. The relocated intermediate depth event hypocenters are shown by small stars. The magenta focal mechanism is the Global Centroid-Moment Tensor (GCMT) solution plotted at the centroid location. The forest green focal mechanism is the composite focal mechanism of the two-faulting slip model at the faulting centroid. Pink focal mechanisms are early GCMT solutions for larger aftershocks.

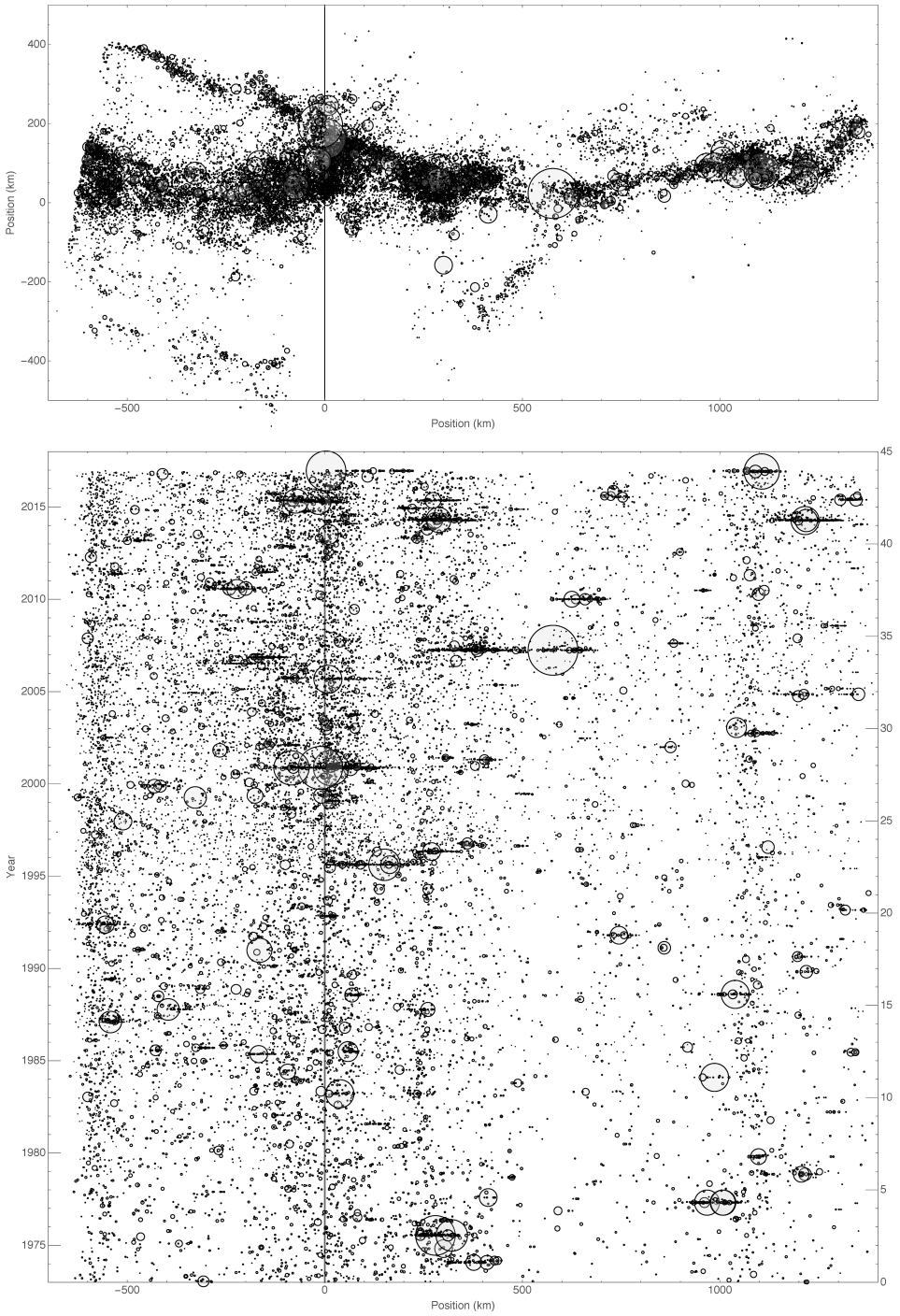

Figure S8. USGS-NEIC seismicity in the New Britain-Solomon Islands trench system with $m_b \geq 4.5$ for the time period 1973 to 2016. The top panel shows the seismicity in map view (area of the circles is scaled proportional to the seismic moment). The reference position at the junction of the trenches is along the epicenter of the December 17, 2016 M_W 7.9 event. The time sequence of seismicity is shown below. Note the concentration of seismicity near the trench junction, the sparsity of seismicity in the central Solomon Islands to the east in the vicinity of the great April 1, 2007 M_W 8.1 earthquake, and the concentration of activity in the southern Solomon Islands. Also note the regional tendency for large events to cluster spatially and temporally in 1974, 1975, 1977, 1995, 2000, and 2015.

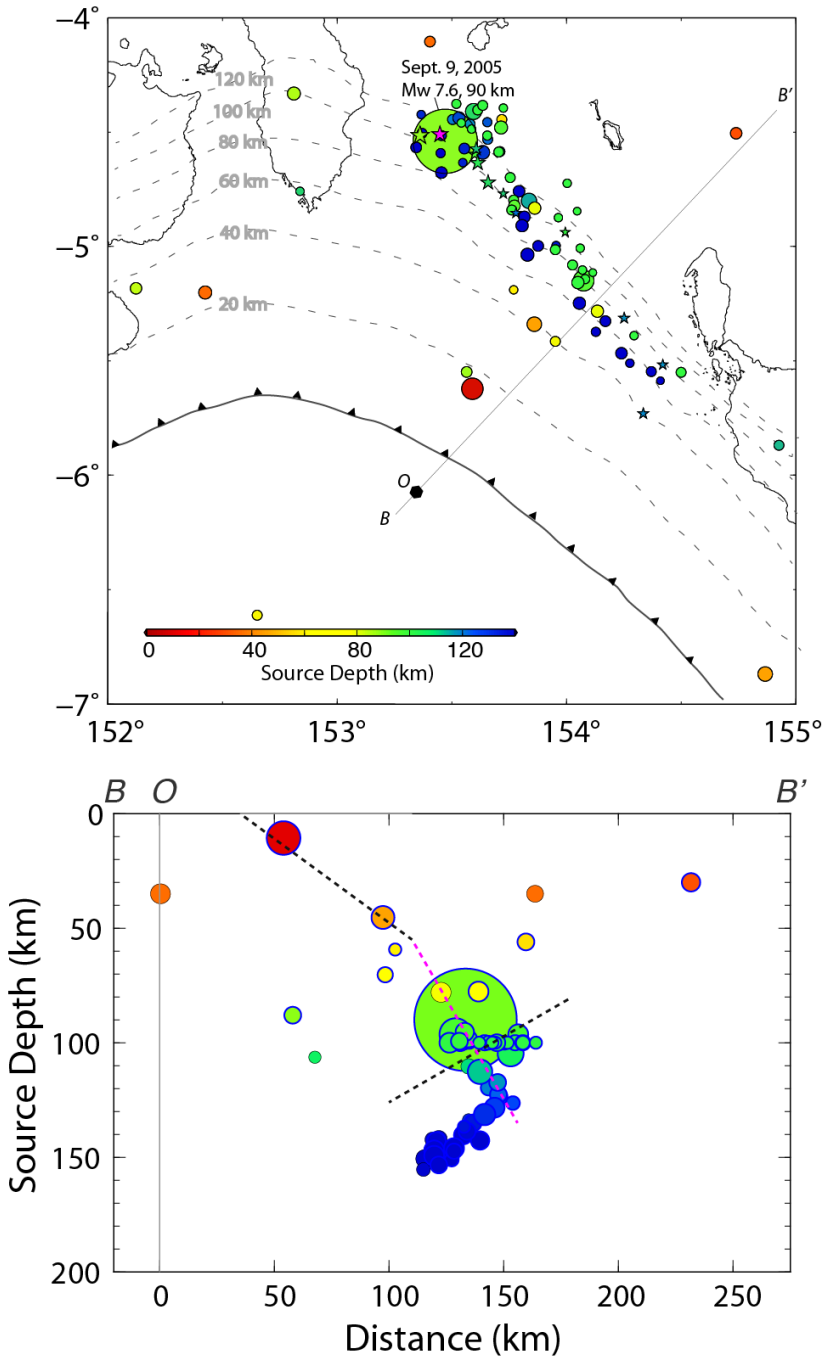

Figure S9. The upper panel shows the first week of aftershocks for the September 9, 2005 M_W 7.6 intraplate rupture with a hypocenter at 90 km (circles). The stars indicate the epicenters of the December 17, 2016 M_W 7.9 earthquake (magenta) and its relocated aftershocks from Figure 2. Note how closely the extent of intermediate depth activity corresponds between the 2005 and 2016 events, and the almost total lack of aftershock activity on the shallow megathrust for 2005, in contrast to 2016 (Figure 2). The lower panel shows a vertical cross-section along the line B-B′, which is the same as in Figure 2, with the positions of the 2005 event and its aftershocks (triangles) shown. The dashed lines are the same planes as in the vertical section in Figure 2. The 2005 event may have activated both 60° and 30° dipping planes within the slab, with the shallow dipping plane parallel to, but 30 km deeper than the rupture plane in 2016.